

A FILTERING APPROACH FOR STATISTICAL INFERENCE IN A STOCHASTIC SIR MODEL WITH AN APPLICATION TO COVID-19 DATA

KATIA COLANERI[✉], CAMILLA DAMIAN[✉], AND RÜDIGER FREY[✉]

ABSTRACT. In this paper, we consider a discrete-time stochastic SIR model, where the transmission rate and the true number of infectious individuals are random and unobservable. An advantage of this model is that it permits us to account for random fluctuations in infectiousness and for non-detected infections. However, a difficulty arises because statistical inference has to be done in a partial information setting. We adopt a nested particle filtering approach to estimate the reproduction rate and the model parameters. As a case study, we apply our methodology to Austrian Covid-19 infection data. Moreover, we discuss forecasts and model tests.

Keywords: Stochastic SIR Model, Nested Particle Filtering, Parameter Inference, Hidden Markov Model, Epidemiological Data.

1. INTRODUCTION

Infectious diseases have key characteristics that simple epidemiological models may not be able to capture. To begin with, the infection or transmission rate may depend on several random factors, such as changes in the infectiousness of the virus, environmental conditions and seasonality, and eventually policy measures. This suggests that the rate should be modelled as a stochastic process. Moreover, there is randomness in the transmission process of a disease, in particular if the population size is small. Finally, many infections are not detected since medical tests might be necessary to confirm a diagnosis. This implies that an analyst is not able to fully observe the components of the epidemiological system; in particular, the transmission rate and the true number of infections are latent.

To account for these characteristics, we develop a stochastic and partially observable SIR model with a random transmission rate. We first frame our model within the setting of a hidden Markov model (HMM). This consists of two components: a latent Markov process (the so-called state process), and an observable process (the so-called measurement or observation process) which is affected by the state, see Elliott et al. (2008) and Churchill (2005) for details. In our specific setup, the state process consists of the compartments of the SIR model and the of transmission rate. The observation process, on the other hand, is given by the number of newly confirmed cases. In a

KATIA COLANERI, DEPARTMENT OF ECONOMICS AND FINANCE, UNIVERSITY OF ROME TOR VERGATA, VIA COLUMBIA 2, 00133 ROME, ITALY. CORRESPONDING AUTHOR.

CAMILLA DAMIAN, INSTITUTE OF STATISTICS AND MATHEMATICAL METHODS IN ECONOMICS, TU WIEN, WIEDNER HAUPTSTR. 7, 1040 VIENNA, AUSTRIA

RÜDIGER FREY, INSTITUTE FOR STATISTICS AND MATHEMATICS, VIENNA UNIVERSITY OF ECONOMICS AND BUSINESS, WELTHANDELPATZ 1, 1020 VIENNA, AUSTRIA

E-mail addresses: katia.colaneri@uniroma2.it, camilla.damian@tuwien.ac.at, rfrey@wu.ac.at.

second step, we extend our framework to include quarantine measures. This is done by immediately removing the newly confirmed cases from the pool of infectious people. A stochastic epidemiological model with similar features (but without quarantine) has been considered in Stocks et al. (2020a) for the spread of Rotavirus infections in Germany.

Statistical inference for this type of models is challenging because of noisy observations, as well as randomness and non-linearity in the transmission process. To address this issue, Stocks et al. (2020a) use a frequentist estimation methodology and compute the MLE for the model parameters via the *iterated filtering* approach of Ionides et al. (2015). In this paper, instead, we analyse the problem using a Bayesian approach. Our objective is to approximate the posterior distribution of the state variables and of the model parameters. For this purpose, we rely on sophisticated techniques from stochastic filtering and adapt the nested particle filter of Crisan and Miguez (2018) to our setup. The ensuing algorithm is recursive and can be implemented efficiently. Simulation experiments demonstrate the good performance of this methodology.

Our approach has many advantages. First, because of its Bayesian nature, it is easily adapted if additional sources of information – for example, in our context, sewage data – become available. In a similar spirit, expert opinions on the state of the epidemiological system are readily incorporated into prior distributions. Second, our methodology is ideally suited for forecasting of future infection numbers. This is an important application of epidemiological models, as these forecasts are used to gauge potential stress for the health system and to inform decisions on containment measures. In our context, forecasts are based on the *predictive posterior distribution*, so that parameter uncertainty is taken into account naturally, making the procedure robust. Last, our approach makes it possible to conduct formal goodness-of-fit tests for the predictive distribution.

As a case study, we apply the version of the model with quarantine to Covid-19 infection data from Austria. A comparison with the official estimates of the Austrian health agency AGES shows that our approach produces qualitatively similar results for the *effective reproduction number*. We also discuss an application of our goodness-of-fit tests in the context of Austrian Covid-19 data, which provides further support for our methodology. Summarizing, our results show that statistical inference for an elaborated epidemiological model with partial information is indeed feasible, if one uses recently-developed tools from stochastic filtering.

We continue with a discussion of the relevant literature. To the best of our knowledge, there are only few contributions that treat statistical inference for epidemiological models as an estimation problem under partial information. Hasan et al. (2022) use the extended Kalman filter (EKF) in an SIR model with additional Gaussian noise to analyse Scandinavian Covid-19 data. However, their model dynamics are somewhat implausible; in particular, the effective reproduction number is modelled as a random walk with Gaussian increments and can therefore become negative. Moreover, the SIR model is a non-linear system and the EKF linearizes these dynamics in a somewhat ad-hoc fashion, so that optimality and stability of the estimates cannot be guaranteed (see e.g. Budhiraja et al. (2007)). However, the EKF is comparatively simple and it often works well when non-linearities are small.

Besides Stocks et al. (2020a), a few other interesting papers are Sun et al. (2015) and Corbella et al. (2022). Sun et al. (2015) study parameter estimation for three partially observed dynamical models for the evolution of biological, ecological or environmental processes; namely, a deterministic

model, a Markov-chain-based model and a model described by stochastic differential equations. They address the inference problem using approximate Bayesian computing. In Corbella et al. (2022), an epidemiological system is described via a state-space model, where randomness is used to address relatively rare severe events. The authors use multiple dependent datasets and develop algorithms for parameter inference based on a pseudo-marginal approach.

The rest of the paper is organized as follows. In Section 2 we introduce the model; in Section 3 we describe the nested particle filter; in Section 4 we present results for simulated data; Section 5 is concerned with applications to Austrian infection data; finally in Section 6 we discuss forecasts and model tests. Appendices A, B and C collect, respectively, some comments on nested particle filter, inputs for the simulation study and inputs for the real data analysis.

2. MODEL SPECIFICATION

In the sequel, we introduce a stochastic version of the standard SIR model, where both the actual number of infected people and the infection rate are random and unobservable. Since we will test our methodology on Covid-19 data, our model specifications account for some special features of this context, such as testing and quarantine regulations. We describe the model in two steps. In the first step (Section 2.1), we consider a simpler case in which quarantine is not taken into account, and develop a discrete-time HMM for the epidemiological system. In the second step, we include quarantine. This generates an additional dependence channel between the state variable and the observations that we explain better in Section 2.2.

Notation. We begin by introducing key variables of the model. First, since infection numbers are usually reported on a daily or a weekly basis, we work in a discrete-time setting with time points $(0 = t_0, t_1, \dots, t_n, \dots)$ (in the data analysis, we assume that $t_n - t_{n-1}$ is one day). We consider a population with N individuals and we assume, for simplicity, that the population size stays constant over time.¹ We then let

- S_n be the number of susceptible individuals at time t_n ;
- I_n be the number of infectious persons at time t_n who can generate new infections in the period $[t_n, t_{n+1})$;
- I_n^+ be the number of individuals who get infected in $[t_n, t_{n+1})$;
- P_n be the number of newly *reported* infections (such as positive tests) in the interval $[t_n, t_{n+1})$, where we assume that testing starts at t_1 ;
- I_n^- be the number of individuals who were infectious at t_n but are removed from I_n over $[t_n, t_{n+1})$, for instance since they recovered or, for certain diseases, are in quarantine;
- R_n be the number of so-called *removed* individuals; that is, people who are either immune or in quarantine at time t_n ;
- Ψ_n be the logarithmic transmission rate; roughly speaking, $\beta_n := \exp(\Psi_n)$ is the expected number of people that are infected by a single infectious person in the period $[t_n, t_{n+1})$.

¹This assumption approximates the case where the observation period is short and the number of deaths due to infections is small compared to the population size.

A process is indicated by capital letters without time index, e.g. S denotes the discrete-time process $(S_n)_{n=0,1,\dots}$. We will also use the notation $P_{1:n}$ to indicate the the history of the process up to n , that is the sequence of random variables P_1, \dots, P_n . Finally, we adopt the usual convention that upper case letters are random variables and lower case variables are data points or samples.

2.1. Step 1: an HMM for epidemics without quarantine. In what follows, we deal with a set of variables, called the *stock* variables, that represent the number of people in each compartment at time t_n , given by (S_n, I_n, R_n) . These, together with the logarithmic infection rate Ψ_n , form the unobservable state. There is also a set of so-called *flow* variables, given by (I_n^+, I_n^-, P_n) , that are used to represent the changes in the stock variables from t_n to t_{n+1} . Among flow variables, I_n^+ and I_n^- are latent, whereas P_n provides the observation.

2.1.1. The state variables. In this section we describe the evolution of the state of system, namely the dynamics of processes (S, I, R) and Ψ . Throughout, we fix a distribution for I_0, R_0 and Ψ_0 . We begin with the logarithmic transmission rate. We assume that Ψ follows a first-order autoregressive process with the dynamics

$$\Psi_n = \Psi_{n-1} + \kappa(\mu - \Psi_{n-1}) + \sigma Z_{n-1}, \quad n = 1, 2, \dots \quad (2.1)$$

for a sequence of independent standard normal random variables $\{Z_n\}_{n=0,1,\dots}$ and parameters $\kappa, \sigma > 0$ and $\mu \in \mathbb{R}$.

Next, we introduce the dynamics of S, I and R . By definition, the number of susceptible people satisfies

$$S_n = N - I_n - R_n, \quad n = 0, 1, \dots,$$

so that S_n can be identified from I_n and R_n (for this reason, we can omit S_n in the set of state variables). The process I evolves according to

$$I_n = I_{n-1} + I_{n-1}^+ - I_{n-1}^-, \quad n = 1, 2, \dots$$

The new infections I_n^+ are modelled as a Poisson random variable,

$$I_n^+ \sim \text{Poisson}(\lambda_n) \quad \text{with } \lambda_n = \beta_n I_n \frac{S_n}{N}, \quad n = 0, 1, \dots, \quad (2.2)$$

where $\beta_n = \exp(\Psi_n)$. The model states that the expected number of new infections is proportional to the number of infectious people and to the fraction of susceptible individuals in the whole population. The proportionality factor β_n gives the average number of people that are infected in $[t_n, t_{n+1})$ by one infectious person in a population where everyone is susceptible, hence it is named *infection* or *transmission* rate.

Remark 2.1. We now briefly comment on our assumptions on the transmission model.

- (i) It is natural to assume that, for small $t_{n+1} - t_n$, the quantity $\beta_n \frac{I_n}{N}$ is small. In that case, we can interpret it as the probability that a susceptible person at time t_n gets infected over the interval $[t_n, t_{n+1})$. If, moreover, infection events are assumed to be independent across susceptible individuals, and the susceptible population S_n is large, then we can use the Poisson approximation to justify the model (2.2).

- (ii) To motivate the assumption for the infection rate dynamics (2.1), we observe that this process is stationary and mean-reverting around the value μ , which is a common behaviour for both endemic and pandemic diseases. In fact, the infection rate of an endemic disease is stationary by definition, whereas, for pandemics, stationarity is often enforced by policy measures. For instance, in the pandemic phase of Covid-19, many European governments tightened containment rules in periods of high infection numbers (corresponding to high values of the reproduction index \mathcal{R}_n , see below) and loosened measures after infection numbers had fallen to more sustainable levels.

Infectious people who are not detected move to the removed state upon recovery from the infection. Thus, at the end of the time interval $[t_n, t_{n+1})$, the number of infectious people is reduced by

$$I_n^- = \gamma I_n, \quad n = 0, 1, 2, \dots,$$

where $\gamma > 0$ is the inverse of the average time a non-detected individual stays infectious. Finally, we assume that

$$R_n = R_{n-1} + I_{n-1}^- - \delta R_{n-1}, \quad n = 1, 2, \dots,$$

where the parameter $\delta > 0$ is such that $1/\delta$ is the average time an infected person enjoys immunity. In other words, a removed person loses immunity and becomes susceptible again at rate δ . For instance, $\delta \sim \frac{1}{200}$ says that people who recovered from the virus on average do not get infected again for about 200 time units (days in our case). Summarizing, the dynamics of the system are as follows. For $n = 1, 2, \dots$,

$$\begin{cases} \Psi_n = \Psi_{n-1} + \kappa(\mu - \Psi_{n-1}) + \sigma Z_{n-1} \\ I_n = I_{n-1} + I_{n-1}^+ - I_{n-1}^- \\ R_n = R_{n-1} + I_{n-1}^- - \delta R_{n-1}, \end{cases} \quad (2.3)$$

where $I_n^+ \sim \text{Poisson}(\beta_n \frac{I_n}{N} S_n)$ and $I_n^- = \gamma I_n$ and $Z_n \sim N(0, 1)$. It is clear from (2.3) and (2.1) that the distribution of the triple (I_n, R_n, Ψ_n) can be described in terms of a transition kernel that depends only on $(I_{n-1}, R_{n-1}, \Psi_{n-1})$, therefore forming a discrete-time Markov chain.

2.1.2. The observations. The true number of infectious people is unknown, as this quantity includes asymptomatic infections or infected individuals who have not (yet) taken a test. Since infections are random and unobservable, we cannot observe the infection rate β_n (or equivalently its logarithm, Ψ_n). At any time $n = 1, 2, \dots$, the available information is thus provided by the number of newly reported cases P_n , whereas all other variables that are used to identify the state are latent. To describe the dynamics of new cases, we assume that an infectious person at time t_n is detected in the interval $[t_n, t_{n+1})$ with probability $q \in [0, 1]$. The parameter q accounts for the availability and reliability of tests and/or for the intensity of public screening programs. We assume that testing occurs independently across infected people and starts at time t_1 . In that case, the conditional distribution of positive tests at time t_n , given the number I_n of infectious people at time t_n , is binomial with parameters I_n and q . That is to say,

$$P_n \sim \text{Binomial}(\lfloor I_n \rfloor, q), \quad n = 1, 2, \dots$$

where $\lfloor \cdot \rfloor$ denotes the floor function. Formally, at any time t_n , the available information can be described by the history $P_{1:n}$.

Note that other data sources, such as results from sewage screening or sentinel systems, are easily integrated into our approach, provided that the conditional distribution of these variables given I_n is known (however, this is left for future research).

2.2. Step 2: an extension with quarantine. In this section, we consider an extension of the model in Step 1, where quarantine is introduced. This, in turn, implies a modification in the dynamics of removed individuals; that is, we assume that a person who tests positively is immediately removed from the pool of infectious people to reflect quarantine measures or self-isolation precautions. In addition, infectious people who are not detected move to the removed state upon recovery from the infection, as before. Thus, for any $n = 0, 1, 2, \dots$, the number of infectious people is reduced by

$$I_n^- = P_n + \gamma I_n,$$

where we set $P_0 = 0$ as we assumed that testing starts at time t_1 .² In summary, the dynamics of the system are as follows. For $n = 1, 2, \dots$,

$$\begin{cases} \Psi_n = \Psi_{n-1} + \kappa(\mu - \Psi_{n-1}) + \sigma Z_{n-1} \\ I_n = I_{n-1} + I_{n-1}^+ - I_{n-1}^- \\ R_n = R_{n-1} + I_{n-1}^- - \delta R_{n-1}, \end{cases} \quad (2.4)$$

where $I_n^+ \sim \text{Poisson}(\beta_n \frac{I_n}{N} S_n)$, $I_n^- = P_n + \gamma I_n$, $P_n \sim \text{Binomial}([I_n], q)$ and $Z_n \sim N(0, 1)$. As before, the observations are given by the history of confirmed cases, $P_{1:n}$ for every $n = 1, 2, \dots$.

In the following statistical analysis we use the property that the triple (I, R, Ψ) is conditionally Markovian, given the observations, which is due to the fact that (I, R, Ψ, P) is Markovian. Moreover, note that the state variables in the model with quarantine cannot be described independently of the observations, which directly appear in their dynamics. Therefore, this model no longer falls into the class of standard HMMs.

Reproduction rate. The effective reproduction rate \mathcal{R}_n is an index that measures the number of individuals who are infected, on average, by a specific infectious person, given the state of the pandemic system at time t_n . To identify \mathcal{R}_n in the model with quarantine,³ note first that an infected individual transmits the disease, on average, to $\beta_n S_n / N$ people per day. Moreover, the time that elapses before an infected person transits to the compartment of removed individuals, R , is the minimum of τ^{rec} (the time up to recovery) and τ^{quar} (the time until the person tests positively and is put into quarantine). Under our model dynamics, τ^{rec} and τ^{quar} have a geometric distribution with parameter γ and q , respectively. Moreover they are independent, so that $\min\{\tau^{\text{rec}}, \tau^{\text{quar}}\}$ follows a geometric distribution with parameter $\gamma + q - \gamma q \approx \gamma + q$. Hence, the expected time up to removal satisfies $\mathbb{E}(\min\{\tau^{\text{rec}}, \tau^{\text{quar}}\}) \approx (\gamma + q)^{-1}$, and

$$\mathcal{R}_n \approx \frac{\beta_n}{\gamma + q} \frac{S_n}{N}. \quad (2.5)$$

²Note that we use the same notation I_n^- to indicate the number individuals who are removed from the pool of infectious with and without quarantine, but their dynamics are different.

³For the version of the model without quarantine it is known that $\mathcal{R}_n \approx \frac{\beta_n}{\gamma} \frac{S_n}{N}$.

3. STATISTICAL METHODOLOGY

When discussing statistical inference for the model described in Section 2, we can distinguish two problems: the *filtering* problem and the *parameter estimation* problem. The filtering problem is concerned with inferring the state process – in our case, the triple (I, R, Ψ) – conditional on the available observations and on a given parameter vector Θ . The parameter estimation problem, on the other hand, is concerned with the case in which parameters values are also unknown. A straightforward way to estimate state and parameters jointly within a bootstrap filter would be to augment the state space so that it includes a parameter vector as a constant-in-time variable; however, this implies that the parameter space is explored only in the initialization step of the algorithm, making it destined to degenerate, see e.g. Kantas et al. (2015). It is thus important to use a methodology that periodically reintroduces diversity in the parameter space.

Having this in mind, in this paper we chose to adapt the nested particle filtering (NPF) algorithm of Crisan and Miguez (2018) to track the posterior distribution of the (static) unknown parameters in our model, as well as the joint posterior distribution of parameter and state variables, in a recursive fashion. More specifically, the NPF algorithm consists of two nested layers of particle filters: an “outer” filter, which approximates the posterior of Θ given the observations, and a set of “inner” filters, each corresponding to a sample generated in the outer layer and yielding an approximation of the posterior measure of the state conditional on both the observations and the given sample of Θ . In this section, we briefly describe this methodology within our framework, starting with the standard bootstrap filter (conditional on a given parameter sample) for the state which are batched to build the inner layer of the NPF algorithm.

3.1. Inner (State) Filter. The filtering problem is concerned with inferring the state process – in our case, the triple (I, R, Ψ) – conditional on the available observations and on a given parameter vector Θ . Assuming that both the transition density of the state process and the conditional density, at each discrete-time instance, of observation given signal and parameters are known, the goal reduces to tracking the posterior probability distribution of the state and it can be accomplished by standard particle (bootstrap) filtering (see, e.g. Gordon et al (1993)). In what follows, we provide a schematic representation of the bootstrap algorithm in our context.

- (1) *Initialization* ($n = 0$): draw i.i.d. state particles $(i_0^{(m)}, r_0^{(m)}, \psi_0^{(m)})$, $m = 1, \dots, M$ from the prior distribution.
- (2) *Recursive step* (from $n - 1$ to n) Given a total of M state particles (Monte Carlo samples) available at time $n - 1$ and the new observation p_n , at time n :
 - (a) *Propagate*: propagate $(i_{n-1}^{(m)}, r_{n-1}^{(m)}, \psi_{n-1}^{(m)})$ to $(\bar{i}_n^{(m)}, \bar{r}_n^{(m)}, \bar{\psi}_n^{(m)})$, $m = 1, \dots, M$, according to Equation 2.3 (for the no-quarantine model) or Equation (2.4) (for the quarantine model).
 - (b) *Compute normalized weights*: compute particle weights proportional to the binomial likelihood; i.e. we define $a_n^{(m)} = \binom{\bar{i}_n^{(m)}}{p_n} q^{p_n} (1-q)^{\bar{i}_n^{(m)} - p_n}$, and then the normalized weights are given by $\bar{w}_n^{(m)} = \frac{a_n^{(m)}}{\sum_{m=1}^M a_n^{(m)}}$.

- (c) *Resample*: for $m = 1, \dots, M$, let $(i_n^{(m)}, r_n^{(m)}, \psi_n^{(m)}) = (\bar{i}_n^{(j)}, \bar{r}_n^{(j)}, \bar{\psi}_n^{(j)})$ with probability $\bar{w}_n^{(j)}$, $j \in \{1, \dots, M\}$.

3.2. Parameter Estimation via Nested Particle Filtering. When it comes to parameter estimation in our setup, we can distinguish two sets of parameters influencing the epidemiological system. On the one hand, we have the triple $\theta = (\kappa, \sigma, \mu)^\top$, which governs the dynamics of the logarithmic infection rate. On the other hand, we have the rates q , γ and δ . It is worth noticing that our observation process consists only of the number of reported cases and that, due to such limitations in the nature and in the length of the observation time series, we will not be able to estimate all model parameters with reasonable accuracy and we will thus resort to fixing the rates exogenously.⁴ That is, we assume that the parameters q , γ and δ are derived from other data (for instance, different medical data, sewage data, as well as the results of other statistical studies) and hence represent a fixed input of our model. As an example of a study reporting calibrated detection rates for Austria specifically, we refer the reader to Rippinger et al. (2021).

Nested Particle Filtering Algorithm. Next we describe the NPF of Crisan and Miguez (2018), which is used for estimating the posterior distribution of the state variables and of the unknown parameters. To simplify notation, in the following schematic description of the algorithm we denote by $X_n = (I_n, R_n, \Psi_n)^\top$, $n = 0, 1, \dots$, the state variables.

(1) *Initialisation.*

- Draw K independent and identically distributed samples of the parameter vector, $\theta_0^{(k)}$, $k = 1, \dots, K$, from a prior distribution.
- For each parameter configuration $\theta_0^{(k)}$, $k = 1, \dots, K$, draw M independent and identically distributed samples of the state variables, $x_0^{(k,m)}$, $m = 1, \dots, M$, from a prior distribution, so that the total number of particles in the signal space is $K \cdot M$.

(2) *Recursive step.* Let, for $n \geq 1$, $(\theta_{n-1}^{(k)}, x_{n-1}^{(k,m)})$ be the set of available samples at time $n - 1$:

(a) *Jittering and state propagation.* For each $k = 1, \dots, K$:

- (i) Draw parameter particles $\bar{\theta}_n^{(k)} = (\bar{\kappa}_n^{(k)}, \bar{\sigma}_n^{(k)}, \bar{\mu}_n^{(k)})^\top$ by perturbing the available sample using a jittering kernel. We jitter each parameter using a Gaussian distribution truncated on its support with means $\kappa_{n-1}^{(k)}$, $\sigma_{n-1}^{(k)}$ and $\mu_{n-1}^{(k)}$, respectively, and variances ϵ_κ , ϵ_σ , and ϵ_μ , respectively.

- (ii) Conditional on each parameter vector $\bar{\theta}_n^{(k)}$, perform an inner bootstrap filtering step as described in Section 3.1. For each $m = 1, \dots, M$, propagate $x_{n-1}^{(k,m)}$ to $\bar{x}_n^{(k,m)}$ and compute the corresponding (binomial) likelihood $a_n^{(k,m)}$ and normalized likelihood weight $\bar{w}_n^{(k,m)} = \frac{a_n^{(k,m)}}{\sum_{m=1}^M a_n^{(k,m)}}$. For the given $\bar{\theta}_n^{(k)}$, update the corresponding state particles in a standard way (weigh and resample with replacement by means of the multinomial resampling algorithm) to obtain a new set in the signal space, $\tilde{x}_n^{(k,m)}$.

⁴A formal analysis of this issue is given in Stocks et al. (2020b). They show that, for a deterministic SIR model in its endemic (stationary) state, only the infection rate β can be estimated from infection data, while the other SIR parameters have to be estimated from other data sources.

- (b) *Resample parameter particles with replacement.* Compute the approximate the likelihood of each $\bar{\theta}_n^{(k)}$ and the likelihood weight as $w_n^{(k)} = \frac{\sum_{m=1}^M a_n^{(k,m)}}{\sum_{k=1}^K \sum_{m=1}^M a_n^{(k,m)}}$. For each $k = 1, \dots, K$, set $(\theta_n^{(k)}, x_n^{(k,1)}, \dots, x_n^{(k,M)}) = (\bar{\theta}_n^{(i)}, \tilde{x}_n^{(i,1)}, \dots, \tilde{x}_n^{(i,M)})$ with probability $w_n^{(i)}$, $i \in \{1, \dots, K\}$.
- (c) *Approximate the posterior measure.* Approximate the posterior distribution of the parameters by $\mu_n \sim \frac{1}{K} \sum_{k=1}^K \delta_{\theta_n^{(k)}}$, where δ_θ denotes the Dirac measure at point θ .

It is important to note that the first task performed in a given iteration of the algorithm is the *jittering* of existing parameter particles in order to restore diversity in the sample, as such diversity might have been greatly reduced due to a previously occurred resampling step. For further computational details, the reader is referred to Appendix A; moreover, details on inputs and prior choices for the simulation (resp. the data analysis) are given in Appendix B (resp. Appendix C).

4. SIMULATION RESULTS

The goal of this section is to test the previously-described nested particle filtering approach for the model with quarantine restrictions on simulated data that mimic typical features of Austrian Covid-19 data – the *true* parameters used to generate state and observation time series are given in Appendix B. We assumed that the probability of a positive test, the average duration of the illness and the average natural immunity period (i.e. $q, 1/\gamma, 1/\delta$) are given and we fixed them consistently with the values reported by e.g. the Austrian Ministry of Health, see Richter et al. (2020). We ran the simulation for a period of two years (731 days), which is roughly consistent with the length of the real time series used for the application in Section 5. Figure 1, depicts a simulated trajectory of the observation sequence P_n , $n = 1, \dots, 731$. This path shows qualitative properties that are similar to real Covid-19 infection data: for instance, our model naturally generates waves of infections. Note that, towards the end of the simulation period, the number of positive tests becomes low, which affects the accuracy of the estimation of the infection rate and the effective reproduction rate (see also Figure 2 below).

We have used the nested particle filtering approach described in Section 3 to estimate the number of infections, the infection rate $(\beta_n)_{n \geq 1}$, the reproduction rate $(\mathcal{R}_n)_{n \geq 1}$ and the model parameters. The results discussed below have been averaged over 50 independent rounds of the algorithm. Figure 2 displays the true (in black) and filtered (in magenta) trajectory of the effective reproduction rate $(\mathcal{R}_n)_{n \geq 1}$ ⁵. This plot suggests that the true trajectory exhibits higher variance than the filtered one: the filter generally captures the trend of the signal process quite well, but it is not able to detect small movements in a short time interval. Moreover, as mentioned previously, the amount of positive test is quite low towards the end of the simulation period and thus, as the observation process becomes less informative, the accuracy of the filter decreases.

Next, we discuss the estimation of the three unknown model parameters: κ , σ and μ (see the dynamics of $\Psi_n = \log(\beta_n)$ given in equation (2.1)). Their posterior distributions are obtained through the nested particle filtering algorithm and visualized in Figure 3. In each panel, the black line corresponds to the true value of the parameter, the two blue lines to the 5%- and 95%-quantile of the posterior distribution (as obtained by the nested particle filter) and the red line to its mean.

⁵We recommend the reader to use a color (or screen) version of this plot for a better understanding.

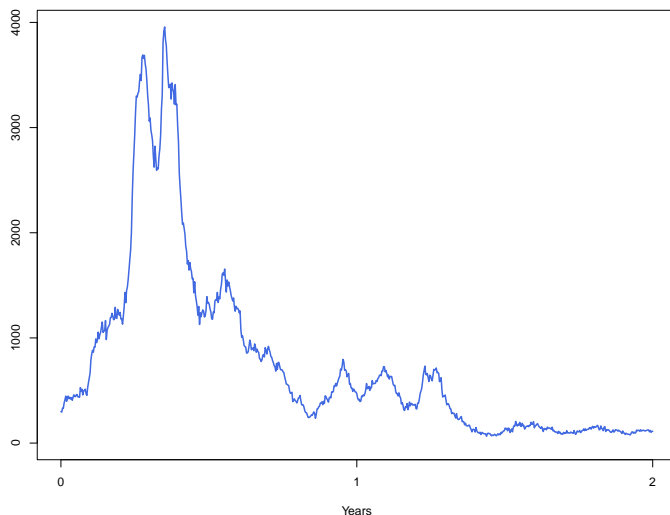


FIGURE 1. Simulated trajectory of the number of positive tests (observation process).

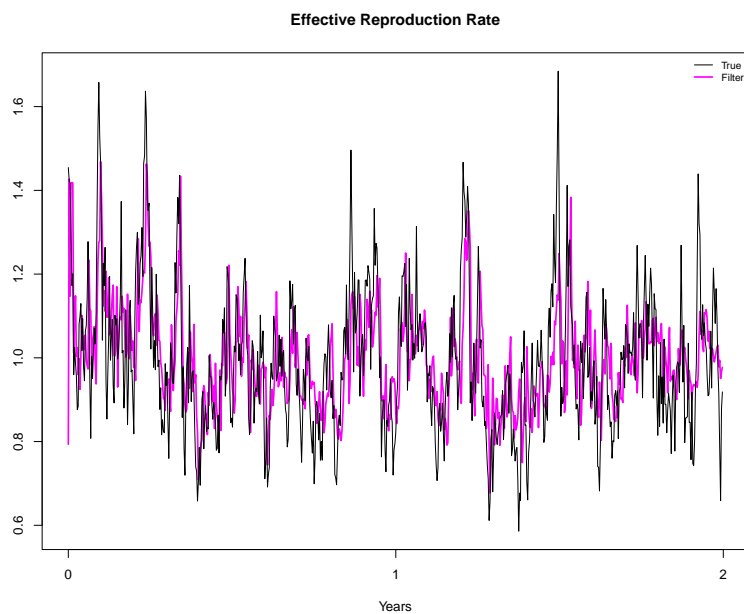


FIGURE 2. True (black) and filtered (magenta) trajectory of the effective reproduction rate.

We can observe how the posterior-mean estimate of μ quickly settles around the true value, while κ and σ seem to be more difficult to estimate. We attribute this difficulty to a couple of reasons. First, we have relatively few observations, corresponding to two years⁶. Second, we considered a

⁶We decided to run our algorithm for two years only to be roughly consistent with the amount of data we used in our case study for the Austrian Covid-19 data.

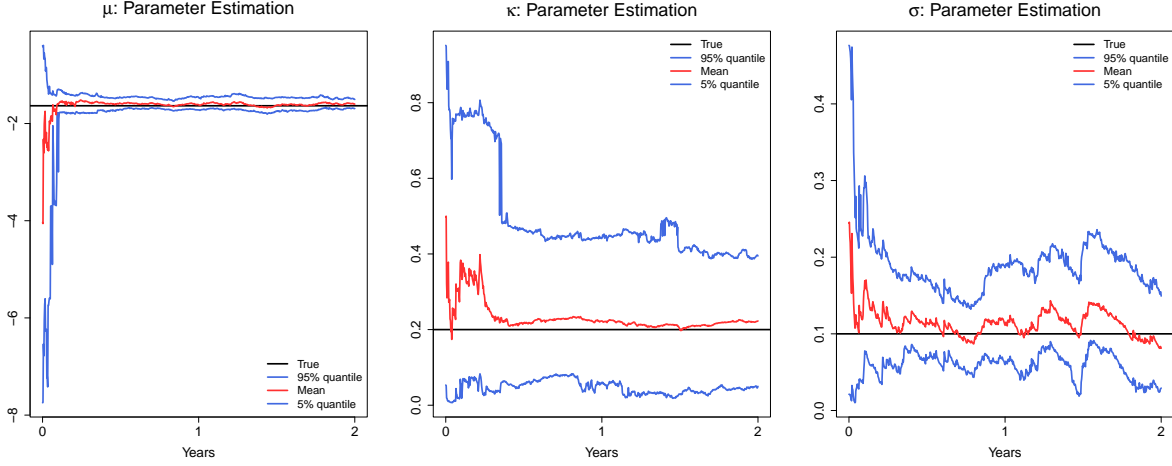


FIGURE 3. Posterior estimates for μ , κ , and σ . The black line corresponds to the true value of the parameter, the two blue lines to the 5%- and 95%-quantile of the posterior distribution (as obtained by the nested particle filter) and the red line to its mean.

quite small support for these parameters, within which it might be more challenging to further discriminate between plausible values in a short time span. Nevertheless, the algorithm is able to detect parameter magnitudes quite rapidly. Moreover, note that there might be a ‘compensatory’ effect at play between posterior-mean estimates for σ and κ , since the long-run variance of Ψ_n is $\sigma^2/2\kappa$, and their distinct impact on state and observations might be decoupled by the algorithm only over a longer time horizon. The mean relative errors between true values and posterior-mean estimates, averaged over the 50 independent runs of the algorithm, are plotted in Figure 4 and they appear consistent with our considerations: in particular, one can compare the behavior of parameter estimation errors for κ and σ with those for the ratio $\sigma^2/2\kappa$. Estimation errors for μ decrease quickly, as expected.

Finally, we carried out robustness checks to ensure that small changes in the parameters q and γ do not affect our estimates too strongly, and we observed that the filtered effective reproduction rate corresponding to slightly-varied values of these parameters presents very similar qualitative and quantitative characteristics.

5. EMPIRICAL RESULTS

In this section, we apply the nested particle filtering approach to Austrian Covid-19 data from May 1, 2020 to June 15, 2022⁷. We did not include further data, as this would have meant to consider earlier and later periods of the pandemic in which policy measures to contain the virus (such as quarantine regulations) and testing behavior of the Austrian population were substantially different. Figure 5 shows the positive tests recorded over these two years. Note that we used a seven-day rolling average of confirmed cases to avoid weekly seasonality effects, such as the fewer tests performed over the weekend. We have set the exogenous parameters (q, γ, δ) and the hyperparameters of the particle filter algorithm according to the values in Appendix C.

⁷The data used for this analysis are publicly available from the AGES website <https://covid19-dashboard.ages.at/>

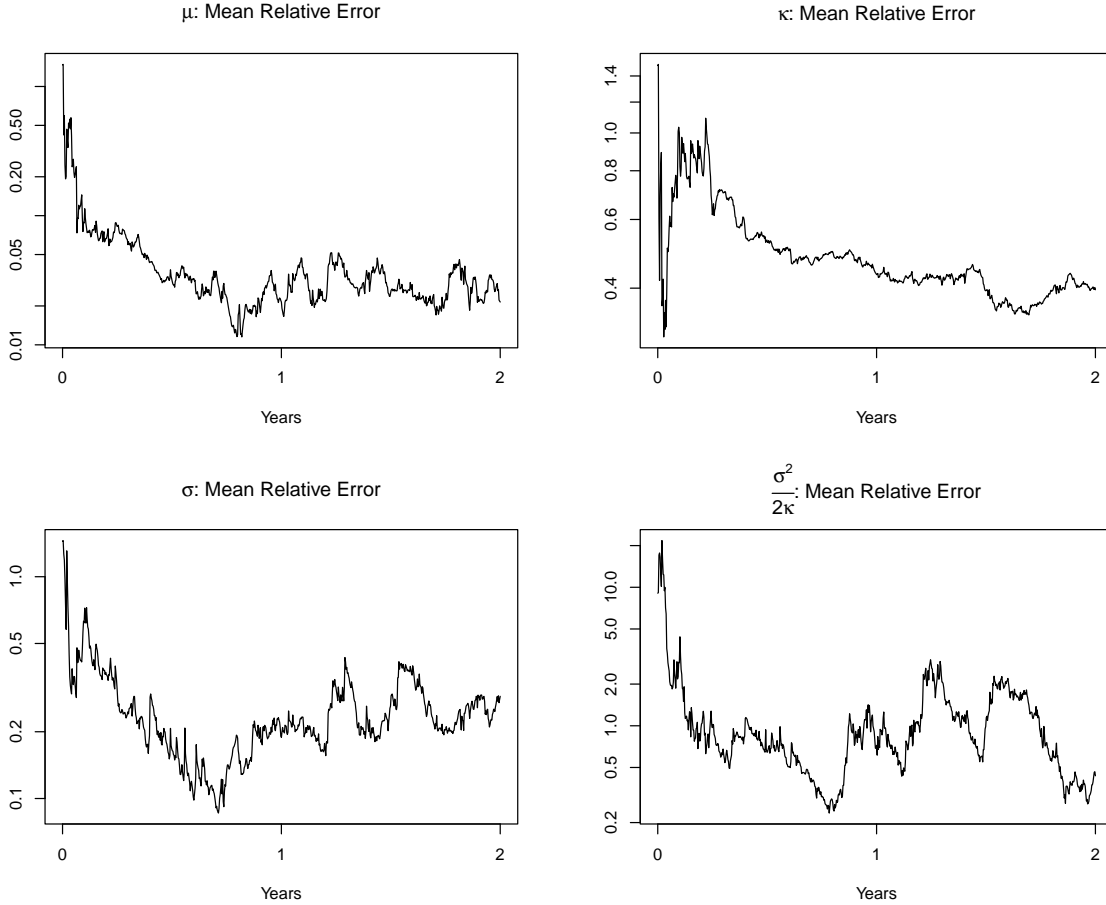


FIGURE 4. Mean relative errors for μ (top left panel), $\sigma^2/2\kappa$ (top right panel), κ (bottom left panel) and σ (bottom right panel), on a logarithmic scale.

We begin with the filtered estimate of the infection rate $(\beta_n)_{n \geq 1}$, which is provided in Figure 6. Here, we observe an upward trend from the beginning of 2022, which is most likely due to the arrival of an highly contagious virus variant (Omicron).

Next, we focus on the effective reproduction rate $(\mathcal{R}_n)_{n \geq 1}$, see equation (2.5). In Figure 7, we compare our filtered estimates (in magenta) with the official estimate published by the Austrian health agency AGES (in black). The latter is computed using a simple Bayesian model with Gamma-distributed prior for β and Poisson observations, see Richter et al. (2020) for details (see also the supplementary material of Cori et al. (2013) for a description of the methodology). The plot shows that the qualitative behaviour of both estimates is very similar; however, our filtered estimate exhibits more variability and higher spikes, particularly starting from mid-2021. This seems to suggest that our filter reacts faster to changes. Note that, while the infection rate β in the first half of 2022 is persistently higher than in 2021 (cf. Figure 6), the effective reproduction rate displays a spike at the beginning of 2022 and then immediately settles again around one. This is due to the counteracting effect that a large part of the population got infected in a small time window

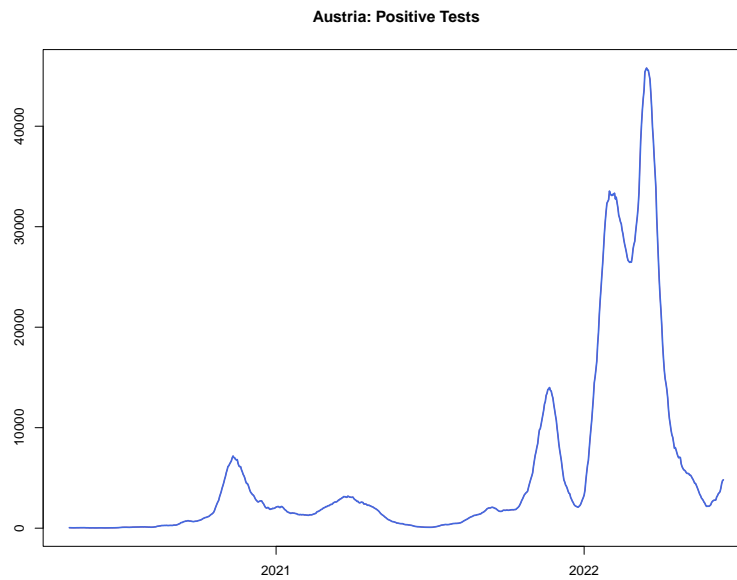


FIGURE 5. Confirmed cases of Covid-19 in Austria (from May 1, 2020 to June 15, 2022).

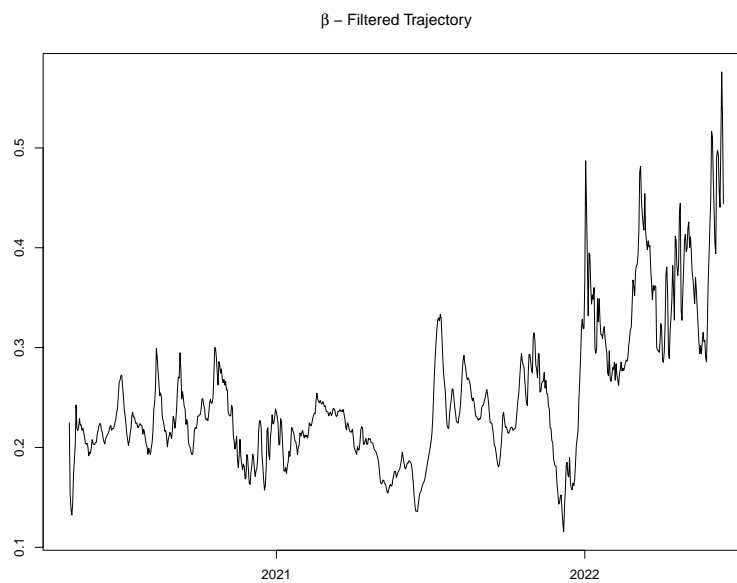


FIGURE 6. Estimates for the infection rate β from Austrian Covid-19 data (from May 1, 2020 to June 15, 2022).

due to higher contagiousness of the Omicron variant, which reduced substantially the number of susceptible individuals.

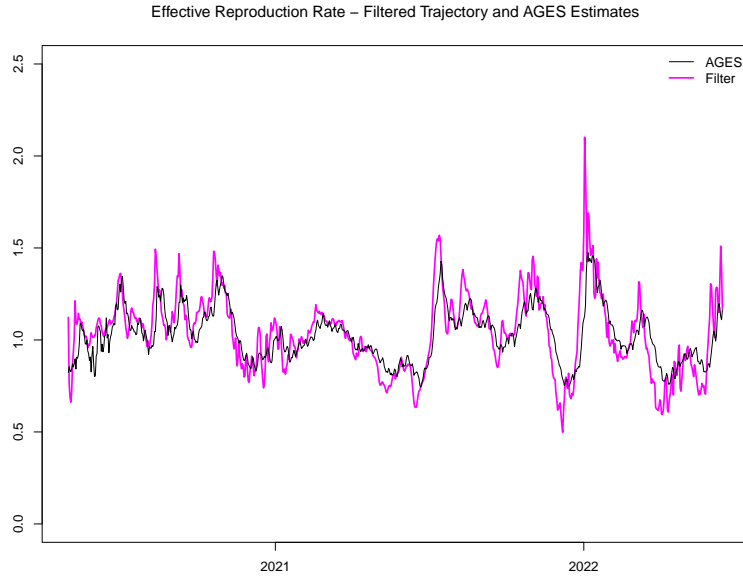


FIGURE 7. Estimates for the effective reproduction rate from Austrian Covid-19 data (from May 1, 2020 to June 15, 2022): in magenta the filtered estimate of \mathcal{R}_n using our methodology; in black the estimate published by the Austrian health agency AGES.

Figure 8 shows how, over time, the posterior distribution concentrates around a specific value $\theta = (\kappa, \sigma, \mu)$. In line with the results from the simulation study, we observe that the posterior-mean estimate of the parameter μ fluctuates the least. Notice that, from the beginning of the second year of data, the posterior-mean estimate of μ seems to increase. This effect may suggest that parameters are, in reality, time-varying (in particular, the arrival of new virus variants might have started a new regime). However, we need to be careful with such conclusions, since our previously-conducted simulation study revealed the limitations in the accuracy of estimates obtained using a relatively short observation series. One possible way to investigate our conjecture is to split the data in two periods – each potentially corresponding to a different regime – and perform parameter inference separately in both to compare estimates; however, this would further restrict the amount of available data, strongly worsening the accuracy and reliability of the resulting estimates and making this approach *de facto* unfeasible for this case study.

6. FORECASTING AND MODEL TESTS

A key application of an epidemiological model is to make forecasts regarding the development of infection numbers, which are used to gauge potential stress for the health system and which serve as a basis for decisions on containment measures. Moreover, analyzing the quality of model-based predictions represents a natural way of testing a given model. Therefore, in this section, we discuss forecasts and model tests for our setup.

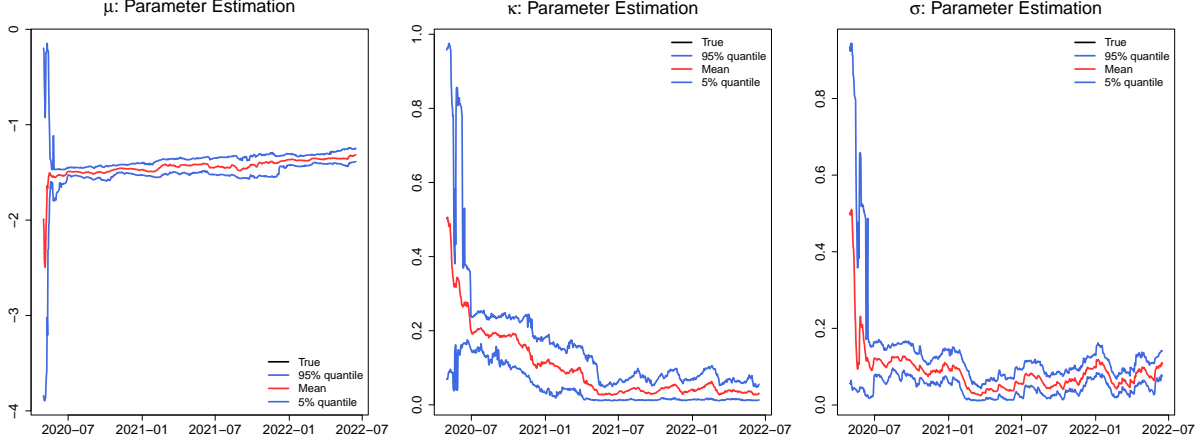


FIGURE 8. Posterior estimates for μ , κ , and σ . The black line corresponds to the true value of the parameter, the two blue lines to the 5%- and 95%-quantile of the posterior distribution and the red line to its mean.

6.1. Methodology. The key quantity for forecasting and testing is the *predictive distribution* of future positive tests over a time horizon Δ , with distribution function

$$F_{n,\Delta}(x) = \mathbb{P}(P_{n+\Delta} \leq x \mid \mathcal{F}_n).$$

To compute an estimate $\hat{F}_{n,\Delta}$ of $F_{n,\Delta}$, we rely on simulations: we first run the particle filter over the period $[0, t_n]$, which provides an approximation of the conditional distribution of the state variables and the model parameters given \mathcal{F}_n . We then draw realisations of I_n, R_n, ψ_n and of the parameters μ, κ, σ from that distribution, which we use to generate trajectories of I, R, ψ and P over the horizon $t_n, \dots, t_n + \Delta$ using the dynamics (2.3) and (2.1).

There are various ways to generate *point forecasts* from the predictive distribution. It is natural to use elicitable forecasts (forecasts minimizing a suitable scoring function), such as the median, higher quantiles or the mean. Now, in our setup the predictive distribution is skewed with a very heavy upper tail (see next paragraph) and the mean is quite unstable. This suggests the use of quantile-based forecasts.⁸

We fix some horizon Δ and consider non-overlapping prediction dates $t_{n_1}, t_{n_2}, \dots, t_{n_m}$, where $t_{n_j} = t_{n_1} + j\Delta$. Then formal *statistical tests* of our methodology can be based on the following classical result of Rosenblatt (1952): if the predictive distribution is correctly specified, that is $\hat{F}_{n_j,\Delta} = F_{n_j,\Delta}$ for all j (this is the null hypothesis for our model test), then, the random variables $\hat{U}_j := \hat{F}_{n_j}(P_{n_j+\Delta})$, $1 \leq j \leq m$, are independent and identically distributed standard uniform⁹.

⁸Since underestimating future infection numbers has more adverse consequences than overestimating them, one might want to work with higher quantiles such as the 75%-quantile instead of the more commonly used median.

⁹Strictly speaking, this is true only if $\hat{F}_{n,\Delta}$ is continuous. In our setup P_n is conditionally binomial and $\hat{F}_{n,\Delta}$ is computed by simulation, therefore it is discrete. However, the number of simulations used is large and the conditional distribution of P_n is very well approximated by a normal, so that under the null hypothesis the distribution of $\hat{F}_{n,\Delta}(P_{n+\Delta})$ is very close to a standard uniform distribution.

This result is the basis for a multitude of statistical tests; for instance, see Gordy and McNeil (2020). Simple tests use *quantile exceedances*. Fix $\alpha \in [0, 1]$. Then, the sequence of quantile exceedances

$$I_{n_j}^\alpha = 1_{\{P_{n_j+\Delta} > q_\alpha(\widehat{F}_{n_j, \Delta})\}}, \quad 1 \leq j \leq m,$$

consists of independent and identically Bernoulli-distributed random variables with $p = 1 - \alpha$. That implies that the number of exceedances $M^\alpha = \sum_{j=1}^m I_{n_j}^\alpha$ has a binomial distribution with parameters m and $p = 1 - \alpha$, which can be tested with a simple binomial test.

More generally, one may test several quantile exceedances jointly by means of *multinomial tests* as explained below (see also Kratz et al. (2018)). Fix quantile levels $0 = \alpha_0 < \alpha_1 < \dots < \alpha_l < \alpha_{k+1} = 1$. For $0 \leq l \leq k$, denote by

$$M^{[\alpha_l, \alpha_{l+1}]} = \sum_{j=1}^m 1_{\{q_{\alpha_j}(\widehat{F}_{n_j, \Delta}) \leq P_{n_j+\Delta} < q_{\alpha_{j+1}}(\widehat{F}_{n_j, \Delta})\}}$$

the number of visits of $P_{n_j+\Delta}$ to the interval $[q_{\alpha_j}(\widehat{F}_{n_j, \Delta}), q_{\alpha_{j+1}}(\widehat{F}_{n_j, \Delta})]$ for all $1 \leq j \leq m$, or, equivalently, the number of visits of $\{\widehat{U}_{n_j}, 1 \leq j \leq m\}$ to the cell $[\alpha_l, \alpha_{l+1})$. It follows that the $k + 1$ -dimensional random vector $(M^{[\alpha_0, \alpha_1]}, \dots, M^{[\alpha_k, \alpha_{k+1}]})$, has a *multinomial* distribution with probabilities $p_1 = \alpha_1, p_2 = \alpha_2 - \alpha_1, \dots, p_{k+1} = 1 - \alpha_k$, which can be tested with goodness of fit tests such as the exact multinomial test, see Menzel (2021).

6.2. Empirical results. We now apply these ideas to the Austrian Covid-19 data. We consider horizons up to 14 days, as this is a common forecasting horizon¹⁰. The parameters of the model and the settings for the nested particle filtering algorithm are given in Appendix C.

Predictive distribution. In Figure 9, we plot several quantiles of $\widehat{F}_{n, \Delta}$ for $\Delta = 1, 2, \dots, 14$ together with the actually observed positive tests for two different prediction dates t_n . The left plot shows the forecasts made on December 23, 2021 – that is, shortly before the start of the Omicron wave in Austria – while the right plot shows the forecasts from January 20, 2022. Since the predictive distribution is very skewed, we use a logarithmic scale for the quantiles. The strong skewness of the predictive distribution can also be seen from Table 1, where we report numerical values of various quantiles and of the mean of $\widehat{F}_{n_j, 14}$ for these two prediction dates.

Looking at the plot on the left, we see that the model predicts the decline of the Delta wave well, but the high infection numbers caused by the onset of Omicron are close to the 90% quantile of the predictive distribution. This is to be expected: since our model is informed only by observations of past positive tests, it is not “aware of” the emergence of a new virus variant. Such information would need to be entered manually by the epidemiologist, for instance as an artificial upward shift in the distribution of the infection rate at t_n . The right plot shows that by January 20, 2022, the model has learned the different regime and actual cases are between the median and the 75% quantile of $\widehat{F}_{n, \Delta}$. However, even on December 20, the infection numbers of the Omicron wave are below the 90% quantile of the predictive distribution, and thus well within the range of possible future scenarios generated by our model.

¹⁰For instance, Bicher et al. (2020) also consider prediction horizons of one and two weeks.

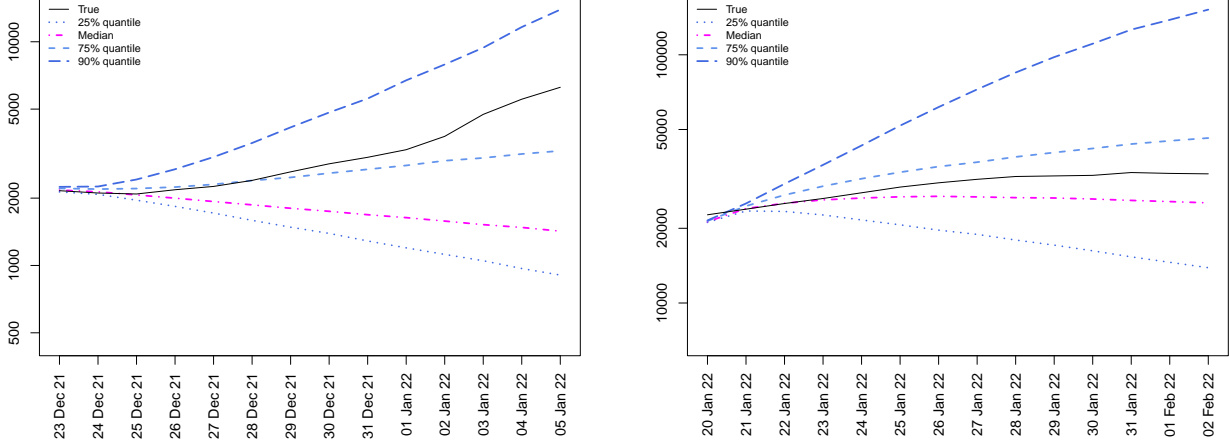


FIGURE 9. Left: quantiles $q_\alpha(\hat{F}_{n,\Delta})$, $\alpha = 0.25, 0.5, 0.75, 0.9$, of $\hat{F}_{n,\Delta}$ for the prediction date $t_n = 23/12/2021$ and prediction horizon Δ between one and 14 days together with the actually observed positive tests; right quantiles and mean of of $\hat{F}_{n,\Delta}$ and realized positive tests for $t_n = 20/01/2022$.

Prediction Date	10%	25%	50%	75%	90%	95%	Mean
Dec 23, 2021	494	851	1411	3509	16338	79142	20194
Jan 20, 2022	8388	13372	24845	46603	155557	248978	56468

TABLE 1. Quantiles and mean of the predictive distribution $\hat{F}_{n,14}$ for two different prediction dates and a horizon of 14 days. Note that the distribution is very skewed with high upper quantiles and a mean exceeding the the 90% quantile (for December 23, 2022) respectively the 75% quantile (for January 20, 2022).

Formal tests. For our tests, we use a horizon of $\Delta = 14$. Since posterior-mean estimates resulting from the nested particle filtering algorithm start stabilising after a little more than a year, we chose September 1, 2021, as the date of the first test, which yields $m = 20$ non-overlapping testing dates. We consider the quantile levels $\alpha_1 = 0.25$, $\alpha_2 = 0.5$, $\alpha_3 = 0.75$, $\alpha_4 = 0.9$ in our tests. In Table 6.2, we report the expected and the observed number of quantile exceedances and cell visits. We see that the quantile exceedances are quite close to their expected value, and a binomial test applied to the observed quantile exceedances yields high p -values (details are omitted). Finally, we ran the exact multinomial test for cell visits and obtained a p -value of 0.521. These test results provide support for the methodology proposed in this paper. Note, however, that the precise outcome of numerical tests varies somewhat with the chosen quantile levels, testing horizon and testing dates. Moreover, the estimated predictive distribution $\hat{F}_{n,\Delta}$ is sensitive to the choice of settings in the nested particle filter, and that some experimentation is therefore necessary (especially given the relatively short series of observations).

Acknowledgements. We are grateful to Sylvia Frühwirth-Schnatter, Luca Gonzato and Giorgia Callegaro for useful comments and suggestions. The work of Katia Colaneri was partially supported

α	0.25	0.5	0.75	0.9	cell	< 0.25	0.25– 0.5	0.5–0.75	0.75–0.9	>0.9
exp.	15	10	5	2	exp.	5	5	5	3	2
obs.	15	11	4	0	obs.	5	4	7	4	0

TABLE 2. Left: expected and observed quantile exceedances; right: expected and observed cell visits.

by project PRIN 2022 “Stochastic control and games and the role of information” (2022BEMMLZ, National PI T. De Angelis, Local Investigator K. Colaneri) funded by the Italian Ministry of University and Research, MUR. Katia Colaneri is also member of Indam-Gnampa. The work of Camilla Damian was partially supported by the Austrian Science Fund project “Detecting gender bias in children’s books”(FWF 1000 Ideas Programme TAI 517-G, PI L. Vana Gür).

Conflict of Interest. The authors have no conflicts of interest to disclose.

APPENDIX A. DETAILS ON THE NESTED PARTICLE FILTERING

Non-Integer Quantities. Note that some quantities in the model described by (2.3) are not integers due to the presence of rates $\gamma > 0$ and $\delta > 0$, while others (e.g. P and I^+) are nonnegative integers by construction. In particular, it might be that the process I , i.e. the number of infectious people, gets below one (or even becomes negative) for some particles at some point in time. To avoid this issue we artificially set $I_n = 0$, whenever a particle is propagated to a negative value. Notice that P_n could be a positive integer even if for some particles $\lfloor I_n \rfloor = 0$. In this case the likelihood of the observation given the particle is zero and hence the particle is eliminated in the resampling.

Computational Details. All computations for this paper are done using R (see R Core Team (2022)). The triple of latent state variables (I, R, Ψ) is stored as a $K \times M \times 3$ array object, where rows correspond to parameter particles, columns to state particles and each $K \times M$ matrix slice along the third dimension corresponds to one of the three state variables. This structure makes the code shorter, readable and relatively efficient, as vectorized operations in R could be used for instance for the state particle evolution. Most importantly, resampling steps can be performed simultaneously along given dimensions of the array.

Although the code is not optimized for speed, and some filtering-specific choices as resampling at each iteration, or jittering every parameter particle, are time consuming, it is relatively fast. One round of the nested particle filter for our application, considering 365 time steps (i.e., one year of data), takes around 1.4 minutes (on the processor AMD Ryzen 7 PRO 4750U).

As computing an estimate for mean relative errors requires averaging over independent runs of the algorithm, we use the package `parallel`; in particular, we use the parallelized analogous of `lapply`, `mclapply`, on 5 cores.¹¹ Overall, it takes about 26 minutes for 50 independent runs of the algorithm for one year of data.

¹¹Note that `mclapply` is not available for Windows, except in the serial sense – that is, resulting in a call to `lapply`, see for instance <https://stat.ethz.ch/R-manual/R-devel/library/parallel/doc/parallel.pdf>.

APPENDIX B. INPUTS FOR THE SIMULATION STUDY

Simulation parameters (true values) and other inputs.

- $q = 10\%$.
- $\gamma = 1/10$.
- $\delta = 1/200 = 0.05$.
- $\kappa = 0.2$.
- $\sigma = 0.1$.
- $\mu = \log(\gamma + q) - \frac{\sigma^2}{2\kappa} \approx -1.63$.
- Number of individuals: $N = 8.917 \cdot 10^6$.
- Number of days: $N^{days} = 731$ (including time 0).
- Time step: $\Delta = t_n - t_{n-1} = 1$ day.
- $R_0 = 0$.

Settings for the nested particle filtering.

- Prior for Ψ_0 : normal with mean μ and standard deviation 0.175.
- Prior for I_0 : gamma (to ensure non-negativity) with mean 3000 and variance 15000.
- Prior for κ , σ and μ : uniform over 1% and 500% of true values.
- Number of particles in the state space $M = 500$ and in the parameter space $K = 500$.
- Variance of the jittering kernels $\epsilon_\kappa = \epsilon_\mu = \epsilon_\mu = 5K^{-2}$.

APPENDIX C. INPUTS FOR THE REAL DATA ANALYSIS

Data characteristics.

- Time period: from May 1, 2020, to June 15, 2022.
- Total number of individuals: $N = 9.028 \cdot 10^6$ (i.e. population of Austria).
- Observations P : 7-day rolling average of confirmed cases.

Fixed parameters and other inputs.

- $q = 10\%$.
- $\gamma = 1/10$.
- $\delta = 1/200 = 0.05$.
- Number of days: $N^{days} = 776$ (including time 0).
- Time step: $\Delta = t_n - t_{n-1} = 1$ day.
- $R_0 = 0$.

Settings for the Nested Particle Filtering.

- Prior for Ψ : normal with mean $\log(\gamma + q) \approx -1.61$ and standard deviation 0.1.
- Prior for I_0 : gamma (to ensure non-negativity) with mean 470 and variance 2350, where the mean corresponds to \bar{p}/q and $\bar{p} = 47$ to the 7-day rolling average of confirmed cases on the day preceding the start of our data analysis (i.e. on April 30, 2022).
- Prior for κ : uniform over $[0.01, 1]$. This prior is chosen to be uninformative.
- Prior for σ : uniform over $[0.01, 1]$ (uninformative).

- Prior for μ : uniform over $[-4, -0.01]$ (uninformative).
- Number of particles in the state space $M = 600$ and in the parameter space $K = 600$.
- Variance of the jittering kernels $\epsilon_\kappa = \epsilon_\mu = \epsilon_\mu = 5K^{-2}$.

REFERENCES

- M. Bicher, M. Uba, L. Rainer, F. Bachner, C. Rippinger, H. Ostermann, N. Popper, S. Thurner, and P. Klimek. Supporting Austria through the COVID-19 epidemics with a forecast-based early warning system. MedRxiv, <https://doi.org/10.1101/2020.10.18.20214767>, 2020.
- A. Budhiraja, L. Chen, and C. Lee. A survey of numerical methods for nonlinear filtering problems. *Physica D: Nonlinear Phenomena*, 230(1-2):27–36, 2007.
- G. A. Churchill. Hidden Markov Models. *Encyclopedia of Biostatistics*, 4:1–8, 2005.
- A. Corbella, A. M. Presanis, P. J. Birrell, and D. De Angelis. Inferring Epidemics from Multiple Dependent Data via Pseudo-Marginal Methods. *arXiv preprint arXiv:2204.08901*, 2022.
- A. Cori, N.M. Ferguson, C. Fraser, and S. Cauchemez. A new framework and software to estimate time-varying reproduction numbers during epidemics, *American journal of epidemiology*, 178(9): 1505–1512, 2013.
- D. Crisan and J. Miguez. Nested particle filters for online parameter estimation in discrete-time state space Markov models. *Bernoulli*, 24:3039–3086, 2018.
- O. Diekmann, H. Heesterbeek, and T. Britton. *Mathematical tools for understanding infectious disease dynamics*, volume 7. Princeton University Press, 2013.
- R. J. Elliott, L. Aggoun, J. B. Moore. *Hidden Markov models: estimation and control*, volume 29. Springer Science & Business Media, 2008.
- M. Gordy and A. McNeil. Spectral backtests of forecast distributions with application to risk management. *Journal of Banking and Finance*, 116, 2020.
- N.J. Gordon, D.J. Salmond and A.F.M. Smith. Novel approach to nonlinear/non-Gaussian Bayesian state estimation. *IEE proceedings F (radar and signal processing)*, 140(2):107–113, 1993.
- A. Hasan, H. Susanto, V. Tjahjono, R. Kusdiantara, E. Putri, N. Nuraini, and P. Hadisoemarto. A new estimation method for COVID-19 time-varying reproduction number using active cases. *Scientific Reports*, 12(1):1–9, 2022.
- E. L. Ionides, D. Nguyen, Y. Atchadé, S. Stoev, and A. A. King. Inference for dynamic and latent variable models via iterated, perturbed bayes maps. *Proceedings of the National Academy of Sciences*, 112(3):719–724, 2015.
- N. Kantas, A. Doucet, S. Singh, J. Maciejowski, and N. Chopin. On particle methods for parameter estimation in state-space models. *Statistical Science*, 30(3):328–351, 2015.
- M. Kratz, Y. Lok, and A. McNeil. Multinomial VaR backtests. *Journal of Banking and Finance*, 88:393–407, 2018.
- U. Menzel. *EMT: Exact Multinomial Test: Goodness-of-Fit Test for Discrete Multivariate Data*, 2021. URL <https://CRAN.R-project.org/package=EMT>. R package version 1.2.
- R Core Team. *R: A Language and Environment for Statistical Computing*. R Foundation for Statistical Computing, Vienna, Austria, 2022. URL <https://www.R-project.org/>.
- L. Richter, D. Schmidt, and E. Stadlober. Methodenbeschreibung für die Schätzung von epidemiologischen Parametern des COVID 19 Ausbruchs Österreich. Working paper, AGES, available from <https://www.ages.at/>, 2020.

- C. Rippinger, M. Bicher, C. Urach, D. Brunmeir, N. Weibrecht, G. Zauner, G. Sroczynski, B. Jahn, N. Mühlberger, U. Siebert, et al. Evaluation of undetected cases during the Covid-19 epidemic in Austria. *BMC Infectious Diseases*, 21(1):1–11, 2021.
- M. Rosenblatt. Remarks on a multivariate transformation. *The Annals of Mathematical Statistics*, 23(3):470–472, 1952.
- T. Stocks, T. Britton, and M. Höhle. Model selection and parameter estimation for dynamic epidemic models via iterated filtering: application to rotavirus in Germany. *Biostatistics*, 21: 400–416, 2020a.
- T. Stocks, T. Britton, and M. Höhle. Model selection and parameter estimation for dynamic epidemic models via iterated filtering: application to rotavirus in Germany: Supplementary material. *Biostatistics*, 21, 2020b.
- L. Sun, C. Lee, and J. A. Hoeting. Parameter inference and model selection in deterministic and stochastic dynamical models via approximate Bayesian computation: modeling a wildlife epidemic. *Environmetrics*, 26(7):451–462, 2015.